Cobalt and Nickel Nanocatalysts Confined inside Halloysite Nanotubes for Selective Hydrogenations

Alejandro Serrano-Maldonado, Jean-Bernard Ledeuil, Lénaïc Madec, Romain Rodrigues, Daniel Pla, Montserrat Gómez

https://doi.org/10.1021/acsanm.4c03715

Cobalt and Nickel Nanocatalysts Confined inside Halloysite Nanotubes for Selective Hydrogenations

Alejandro Serrano-Maldonado,[a] *Jean-Bernard Ledeuil,*[b] *Lénaïc Madec,*[c] *Romain Rodrigues,*[d] *Daniel Pla,*[a*] *Montserrat Gómez,*[a*].

[a] Laboratoire Hétérochimie Fondamentale et Appliquée, UMR CNRS 5069, Université Toulouse 3 – Paul Sabatier, 118 route de Narbonne, 31062 Toulouse Cedex 9, France.

[b] Institut des Sciences Analytiques et de Physicochimie pour l'Environnement et les Matériaux, Université de Pau et des Pays de l'Adour, UMR CNRS 5254, 2 avenue du président Angot, 64053 Pau, France.

[c] Institut des Matériaux Jean Rouxel (IMN), CNRS UMR 6502, Université Nantes, 2 rue de la Houssinière BP32229, 44322, Cedex 3 Nantes, France.

[d] SOPHIM, Rue Pierre-Gilles de Gennes, 04310 Peyruis, France.

KEYWORDS. Nickel and cobalt nanocomposites; halloysite; catalytic hydrogenation; biomass-based compounds; selective nitrile reduction.

ABSTRACT

Innovative cobalt and nickel catalytic materials containing metal nanoparticles immobilized into the inner tubes of pristine halloysite, a naturally occurring nanoclay, and their application in hydrogenation reactions of a large variety of substrates from biomass and industrial wastes are described herein. The catalytic materials with a high metal loading (>24 wt.%) were prepared by a one-pot two-steps procedure in the absence of additional stabilizers, leading to metal nanoparticles essentially confined into the support lumen (constituted of aggregates of small nanoparticles) as a result of the privileged electrostatic interactions between aluminols and metal acetate salts ($Ni(OAc)_2$, $Co(OAc)_2$). Both catalytic materials, **Ni/Hal** and **Co/Hal**, gave different chemoselectivities towards the reduction of unsaturated functional groups (carbonyl, C=C, nitrile) under solvent-free conditions, and thus affording selectively added-value compounds depending on the nature of the metal. In particular, the squalene hydrogenation monitoring permitted to identify the partial hydrogenated products and estimate the partial turnover numbers and frequencies, achieving a cumulative TON of 110 and TOF of 151 h^{-1} using the most active catalytic system, *i.e.* **Ni/Hal**.

1. Introduction

First-row transition metals applied in catalytic reactions represent a foremost research field mainly due to their relatively abundance in comparison with precious metals and distinctive reactivity, promoting complementary transformations in relation to 4d and 5d counterparts (for

recent selected reviews, see: [1-5]). Harnessing the sustainability of «light» metals such as lithium, copper, cobalt or nickel in the context of the current societal energy transition encompasses a number of environmental and technological challenges, namely ongoing efforts in preserving natural resources, developing alternative battery technologies and enhancing recycling capabilities to facilitate their upcycling and further use of these critical materials.[6] In particular, the implementation of efficient and sustainable methodologies to recover cobalt[7] and nickel[8] from spent Li-batteries, together with the advent of nickel- and cobalt-free solid-state and polymer alternatives[9] represents a change of paradigm that ensures not only the sustainability, but also the provisioning of these metals even in the event of a rise in their long-term demand associated to low-carbon industries; the market forecast suggests relatively low prices for the near future amid the three-fold decrease of cobalt prices that occurred in early in 2024, mainly due to oversupply.[10]

The reports involving metal nanoparticles applied in catalysis have exponentially grown since 1980s when the relevance of the size on catalytic reactivity was stressed by the researchers (for a pioneering contribution, see [11]), at first mainly involving noble metals but in the last years an undeniable work in more abundant metals has been devoted (for selected reviews, see: [12-19]). In this frame, selective hydrogenation processes represent a huge interest for both academic purposes and industrial applications ([14, 20, 21]). Among 3d metals, nickel occupies a privileged position in hydrogenation applications, being Ni-Raney (a Ni-Al alloy) largely applied but due to its easy deactivation, instability and hazardous issues a plethora of alternative catalysts has been described in the literature (some of them are commercially available), including well-defined (un)supported nickel nanoparticles[22] (for selected reviews, see: [23-25]). Besides, cobalt-based nanoparticle catalytic materials have been less applied in hydrogenation processes in contrast to its well-known CO-

promoted reactivity (hydroformylation of alkenes,[26] Fischer-Tropsch process[27, 28]), albeit showing lower activity than nickel.

From an application viewpoint, high metal loadings are preferred with the aim of minimizing the total amount of catalytic material employed under catalytic conditions; however, when the metal is present in a relative high proportion to the support, bigger particles are often favored, generally losing their unique catalytic properties. In particular, high Ni loading (50 wt.% and more) catalysts supported on SiO_2[29, 30] or Al_2O_3[31, 32] for industrial applications have classically been prepared via precipitation of nickel hydroxocomplexes in the suspension of the support (homogeneous deposition–precipitation) as reported by Hermans and Geus late in the 60's.[33] Since then, enhanced methodologies have been developed encompassing *in situ* formation of nickel silicates as precursors of Ni nanoparticles ranging from 2-24 nm in size upon reduction (between 450-650 °C), leading to the commercialization of the EuroNi-1 catalyst in the 80's.[34, 35] Furthermore, the effect of high cobalt loading for supported heterogeneous catalyst both on alumina and silica supports has been proven to enhance catalytic activity.[36-38]

Taking into account the prevalence of self-assembled silica-based nanostructures[39, 40] in the quest towards the design of environmentally friendly advanced nanocomposites, the unique nanotubular structure displayed by halloysite, a naturally occurring nanostructured clay, featuring rolled up aluminosilicate layers of 10–15 nm internal lumen diameter with average tube diameter of *ca*. 50 nm and different chemical compositions of the inner/outer surfaces[41] offers excellent means to deposit transition metals (Ru,[42] Ag,[43, 44] Au,[45] Pd,[46] Ni,[47] Co,[48] Ni–CoO,[49] Cu–Ni[50]) either via covalent interactions with the silanol-rich surface providing enhanced stability and distribution of the resulting hybrid materials,[51, 52] or confined into the nanotube lumen cavities through ionic interactions,[53] leading to confinement effects.[54] The development of synthetic methods to gain

control not only on the selective deposition but also over fine-tuning particle size and shape, acting as a template for the growth of transition metal nanoparticles, offers enhanced means to impact the catalytic activity of the resulting composite nanomaterials through metal-metal and metal-support synergistic effects.[55, 56]

In the present contribution, the immobilization of Ni and Co nanoparticles into the lumen of the pristine halloysite nanotubes was successfully accomplished without requiring the presence of additional stabilizers. The as-prepared catalytic materials were efficiently applied in solvent-free hydrogenation reactions of biomass-based substrates (α-pinene, ethyl levulinate, furfural, citral), including substrates coming from industrial wastes, such as squalene from the olive oil production and unsaturated fatty acids from agri-food and sewage industrial wastes, affording added-value products. These original catalysts, **Ni/Hal** and **Co/Hal**, exhibited specific chemoselectivity, allowing in particular the synthesis of primary (**Co/Hal**) or secondary (**Ni/Hal**) fatty amines from the hydrogenation of the corresponding nitriles.

2. Experimental section

The general information related to chemicals and instruments is given in the Supplementary Information.

*2.1. Synthesis of **Ni/Hal** and **Co/Hal***

A round-bottom flask was charged with the desired metal acetate salt $Ni(OAc)_2 \cdot 4H_2O$, 1692 mg, 6.8 mmol; $Co(OAc)_2$, 1200 mg, 6.8 mmol), halloysite (800 mg), EtOH (80 mL) and stirred at room temperature for 3 h until a homogeneous suspension was formed. The solvent was then removed under reduced pressure using a rotary evaporator and dried overnight using a vacuum line to obtain the metal precursor impregnated in halloysite. Then, a freshly prepared solution of $NaBH_4$ (1280

mg, 33.8 mmol, 5 equiv. in respect to metal loading) in EtOH (80 mL) was added dropwise to a dispersion of metal salt-impregnated halloysite in EtOH (10 mL) under constant stirring at room temperature. Upon addition completion, the reaction was stirred at room temperature until no hydrogen release was observed to give a black suspension. The supernatant solution (containing sodium borate salts) was removed via cannula filtration and discarded to obtain preformed metal NPs in halloysite as a black solid. Subsequently, the preformed nanocomposite was transferred to a Fisher-Porter bottle and the system was purged with Ar prior to the cannulation of degassed EtOH (80 mL) under Ar to suspend the solids. The system was then pressurized with H_2 (3 bar) at room temperature and heated at 100 °C (in an oil bath) for 18 h under magnetic stirring. Then, the Fisher-Porter bottle was cooled down to room temperature and depressurized under Ar. A black dispersion was obtained, which was transferred to a Schlenk flask via cannulation under Ar. Solvent was removed via cannula filtration and the solid was dried overnight under vacuum to obtain the halloysite supported catalysts M/Hal (M = Ni, Co). Catalysts were stored in the glovebox prior to use.

2.2. General catalytic hydrogenation procedure

A 4 mL vial was charged with the halloysite-supported catalyst (selected **Ni/Hal** or **Co/Hal** amount as specified in each run), the substrate (1 mmol) and a stirring bar under Ar inside a glovebox. The vial was closed with a septum prior to be taken out of the glovebox and placed inside a 50 mL autoclave (TOP Industrie S.A.S.). The septum of the vial was then removed and the autoclave was immediately purged with Ar at room temperature prior to be charged with H_2 (specified pressure in each run). The autoclave was then placed in a pre-heated aluminum block at the desire reaction temperature on a heating plate equipped with a magnetic stirrer. The reaction

mixture was heated at the selected temperature for the specified reaction time. The aluminum block was then removed, the autoclave was allowed to cool down to room temperature and the remaining hydrogen pressure was smoothly released. The reaction crudes were extracted with 3 x 3 mL of selected solvent (heptane or $CHCl_3$ in the case of nitriles) and the combined organic extracts were filtered through a PTFE filter (0.22 μm) to remove the catalyst. After solvent removal under reduced pressure, 1 equiv. of the selected internal standard (n-dodecane or dimethylsulfone) was added. Analysis by GC-FID or ^{1}H NMR in $CDCl_3$ was performed for the determination of conversion, yield and selectivity. ^{1}H and ^{13}C NMR analyses of all organic products were carried out for characterization purposes without further purification.

Blank control tests in the absence of catalyst were systematically carried out and only unreacted starting materials were recovered in all cases.

2.3. Procedure for catalyst recycling

Following the general procedure for catalytic reactions, the reaction was prepared with the desired amount of catalyst (5 mol%, 9.6 mg for **Ni/Hal**; 10 mol%, 24.2 mg for **Co/Hal**), squalene from olive oil (550 mg) and put under the selected conditions (10 bar H_2, 150 °C for **Ni/Hal**; 40 bar H_2, 200 °C for **Co/Hal**) for 2 h. Taking advantage of the magnetic behavior of catalysts, the reaction crudes were extracted with heptane (3 × 3 mL) using an external magnet to easily separate the catalyst from the supernatant. After solvent removal under reduced pressure, n-dodecane as internal standard was added to organics for the determination of yield and selectivity by GC-FID. The recovered catalyst was dried under vacuum and kept under Ar before each consecutive run. The loading of fresh squalene substrate (550 mg) was done under ambient conditions. ICP-AES analyses of all organic extracts were carried out.

3. Results and discussion

3.1. Synthesis and characterization of the catalytic materials

Nanocomposites materials based on Ni or Co nanoparticles immobilized on pristine halloysite nanotubes were prepared by a one-pot two-steps methodology in the absence of additional stabilizing agents, based on our previously reported methodology;[47, 48] this approach permits to fully reduce the corresponding metallic salts, probably generating metal-hydride nanoparticles, crucial for their catalytic reactivity, as previously proven. From a structural point of view, this methodology led to the confinement of metal nanoparticles into the lumen of the support (constituted of alumina groups), in contrast to what is generally observed with transition metals, where MNPs are adsorbed on the external walls (constituted of silanol groups) of the unfunctionalized halloysite; actually, this strategy represents the first report on the inner immobilization of monometallic metal nanoparticles involving non-noble metals (Scheme 1), other than the bimetallic Ni-Cu nanoparticles in halloysite (for the immobilization of noble metals into the halloysite nanotubes, see [42-46, 57, 58]). From a mechanistic point of view, it seems plausible that in a first stage the adsorption of the molecular metal precursor is preferentially done at the external surface of the halloysite nanotubes (silanols) if it is not polar, *e.g.* $[Ni(cod)]_2$,[47] or $[Co_2(CO)_8]$;[48] or at the internal part (aluminols) for ionic metal precursors, such as the acetate salts used in this work, taking into account the different ionic/covalent nature of silanols (less ionic) *versus* aluminols (more ionic).

Moreover, the as-prepared materials, **Ni/Hal** and **Co/Hal** with high metal content (30.6 wt.% Ni for **Ni/Hal** and 24.3 wt.% Co for **Co/Hal**, as determined by ICP-AES; see Table S1 in the Supplementary Material), enable large-scale applications by minimizing the total mass of the required catalytic material. However, a significantly better immobilization of nickel than cobalt

was observed (92% of Ni and 73% of Co deposition). Furthermore, it is important to highlight that only small amounts of sodium (0.4 wt.%) and boron (0.9 wt.% for **Ni/Hal** and 0.5 wt.% for **Co/Hal**) were detected (arising from $NaBH_4$ used in the synthesis), which reveals the efficiency of the synthetic methodology for obtaining catalytic materials with marginal contamination.

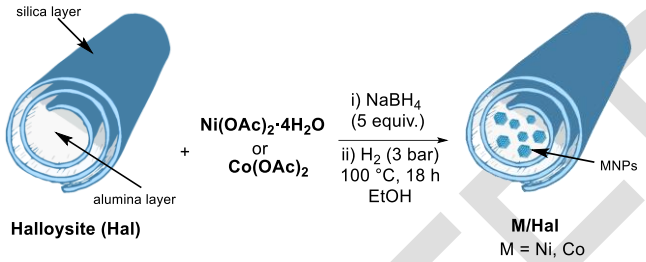

Scheme 1. Synthesis of the catalytic materials **Ni/Hal** and **Co/Hal**, containing Ni and Co nanoparticles confined in the lumen of pristine halloysite (Hal).

FTIR spectra analyses of **Ni/Hal** and **Co/Hal** showed absorption bands in the region of 1650 and 1450 cm^{-1}, indicating the presence of acetate groups coming from the starting metallic salts (see Figures S1-S4 in the Supplementary Information). These anions can not only contribute to the electrostatic stabilization of metal nanoparticles, but also facilitate the immobilization of the metal nanoparticles in the halloysite lumen.[53] Actually, the ionic environment of the lumen mostly constituted of aluminols favors the immobilization of metallic salts (in this case metal acetates) preferentially inside the nanotubes (inner) via electrostatic interactions rather than at silanol outer surface, the latter presenting a more covalent character, in noticeably contrast to the catalytic materials prepared from non-ionic organometallic complexes (such as $[Ni(cod)_2]$ or $[Co_2(CO)_8]$) as metal precursors of MNPs at relative low metal loadings.[47, 48]

Low-resolution Transmission Electron Microscopy (TEM) analyses of the nanocomposite catalytic materials showed that halloysite preserved its nanotube structure, without observing

morphological modifications after metal immobilization (neither by PXRD, see below). Large metal nanoparticles were observed with mean diameters of 8.2 ± 1.7 nm for **Ni/Hal** and 13.2 ± 2.4 nm for **Co/Hal** (Figure 1). The higher load of metal in these materials along with the absence of stabilizers led to considerably larger nanoparticles in comparison with the Ni- and Co-based catalysts previously reported by the group with a load of 5 wt.% Ni (5.3 ± 1.5 nm)[47] and 5 wt.% Co (2.9 ± 0.4 nm in the absence of stabilizer; 3.2 ± 0.9 nm in the presence of CO and quinidine).[48] It is important to mention that the diameter of the halloysite nanotubes was not modified during the synthesis of the catalytic materials (see TEM analyses in Figures S5-S7 of the Supplementary Material).

HAADF-STEM (High-Angle Annular Dark-Field-Scanning Transmission Electron Microscopy) coupled to EDX (Energy-Dispersive X-ray spectroscopy) analyses of **Ni/Hal** and **Co/Hal** showed the presence of the metal along the halloysite nanotubes (Figure 2). With the purpose of verifying that the metal nanoparticles were mainly located in the inner of the nanotubes, TEM images series of a selected area were collected with different tilt angles (see Figure S8 in the Supplementary Information).

To identify the crystalline phases, powder X ray diffraction (PXRD) analyses were performed for both catalytic materials (see Figures S9-S10 in the Supplementary Information). In addition of the crystalline structure of halloysite, Ni(0) and Co(0) crystallographic planes corresponding to *fcc* crystal structures were identified, exhibiting mean crystallite sizes of less than 2 nm for **Ni/Hal** and **Co/Hal**, respectively. The small crystallite size of both nanocomposite materials compared to the size determined by TEM (Figure 1) suggests that the nanoparticles observed by TEM are most likely formed by aggregates of small nanoparticles.

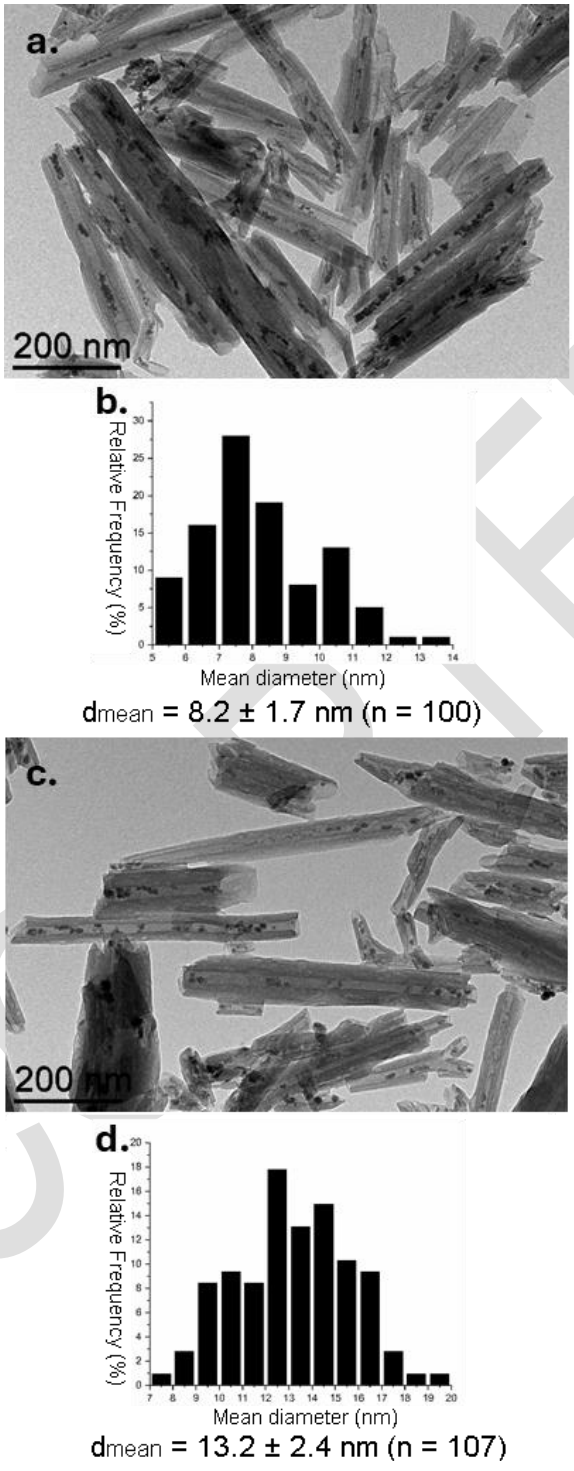

Figure 1. TEM micrographs and size distribution of catalytic materials: a) TEM micrograph of **Ni/Hal**; b) mean diameter and size distribution of **Ni/Hal**; c) TEM micrograph of **Co/Hal**; d) mean diameter and size distribution of **Co/Hal**.

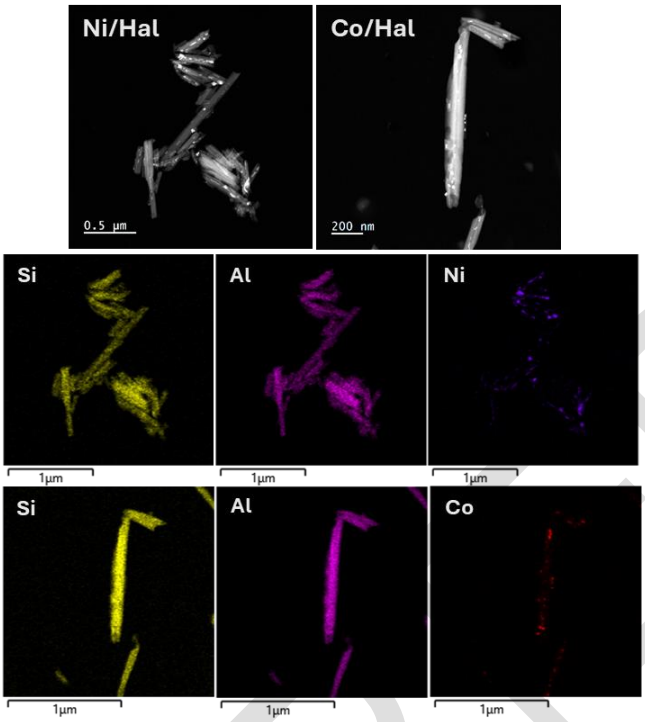

Figure 2. HAADF-STEM images of **Ni/Hal** and **Co/Hal** (top); EDX mapping of Si, Al and Ni for **Ni/Hal** (middle); EDX mapping of Si, Al and Co for **Co/Hal** (bottom).

X-ray photoelectron spectroscopy (XPS) analysis of the as-prepared nanocomposites was performed to determine the elements present on the catalytic materials and the oxidation states of the immobilized metal species. The XPS survey of **Ni/Hal** and **Co/Hal** showed the presence of Si, Al, O, C and Na in agreement with PXRD, FTIR and ICP-AES data (see Figure S11-S12 and Tables S2-S3 in the Supplementary Information). The high-resolution spectrum at the binding region of Ni 2p showed the presence of Ni(0) (45%) and NiO (42%), with 13% of $Ni(OH)_2$ (Figure 3a and Figure S13 in the Supplementary Information), similarly to other Ni-based catalysts prepared by our group.[47, 59, 60] The analysis at the binding region of Co 2p evidenced that the main component was Co(0) (86%), along with 14% of mixed cobalt oxide Co_3O_4 (Figure 3b and Figure S14 in the Supplementary Information), in agreement with previously reported by the group for

CoNPs mainly immobilized on the outer surface of the support.[48] This structural information is crucial for applications in hydrogenation processes, taken into account the low activity observed using Co(II)-based catalytic materials in these processes, as previously proven by our group.[48]

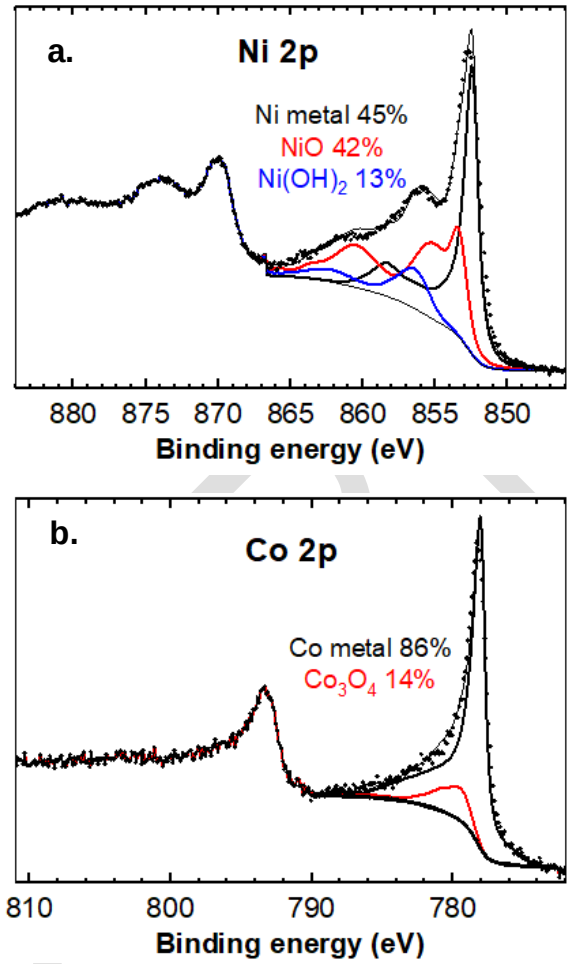

Figure 3. High-resolution XPS spectrum of: a) **Ni/Hal** at the binding region of Ni 2p; black, red and blue continuous traces correspond to Ni(0), NiO and $Ni(OH)_2$ envelopes respectively, used to fit the experimental data (dotted line); the fit was carried out on the Ni $2p_{3/2}$ binding energy; b) **Co/Hal** at the binding region of Co 2p; black and red continuous traces correspond to Co(0) and Co_3O_4 envelopes respectively, used to fit the experimental data (dotted line); the fit was carried out on the Co $2p_{3/2}$ binding energy.

3.2. Catalytic hydrogenations

The novel catalytic materials, namely **Ni/Hal** and **Co/Hal**, were applied in solvent-free hydrogenation processes of a variety of biomass-based substrates, also including waste from sewage and agri-food companies.

We selected a triterpene, squalene (**1**), as benchmark reaction with the aim of comparing the reactivity of the as-prepared catalysts with respect to the commercially available catalysts used on an industrial scale (Ni-Clariant® and Ni-BASF®);[61] the obtained squalane product (**1a**) finds applications as an emollient to soften the skin along with its lipid barrier restoration properties.[62] The raw material comes from an industrial process for extracting squalene from waste edible vegetable oils; it has been further purified in order to remove catalyst poisons (pigments, hydroperoxides…; see the procedure corresponding to the purification of squalene in the experimental section of the Supplementary Information). **Ni/Hal** was active for the conversion of squalene into squalane under relatively smooth conditions, mainly concerning pressure (10 bar H_2, entries 1-2, Table 1). However, at 150 °C even though no squalene is present, squalane only represents ca. 20% of the mixture of products obtained mainly corresponding to those showing partially reduced C=C bonds (entry 1, table 1). At 200 °C and after 4 h, full conversion and selectivity towards squalane was observed (entry 2, Table 1). Lower pressure triggered a dramatic effect on chemoselectivity (only 4% of squalane; entry 3, Table 1). With the aim of reducing the reaction time applying relatively low temperature, the loading of Ni was increased (up to 5 mol%), successfully furnishing squalane (entry 4, Table 1). A GC-FID/MS reaction monitoring of squalene hydrogenation under these conditions (5 mol% Ni loading, 10 bar, and 150 °C) at different times was conducted to evaluate **Ni/Hal** catalyst activity (see Figures S21-S30 in the

Supporting Information). Notably, after 10 minutes the conversion was of 23%, mainly corresponding to one and two C=C bond hydrogenations (in 75 and 17%, respectively; see Table S4 in the Supporting Information). Despite the increasing trend in selectivity towards three and four C=C bond hydrogenations at 20 and 30 min, squalane yield only represented *ca*. 2%. The highest TON observed for one and two C=C bond hydrogenations takes place at 60 min (TON = 13 and 6, respectively), whereas at 75 min the highest TON corresponds to three and four C=C bond hydrogenations (TON = 2.5 and 3.9, respectively). The formation of squalane was significant (*i.e.* hydrogenation of the six C=C bonds) after 75 minutes, reaching a steady-state with a constant TON (20) until reaction completion at 120 min; after 90 min, the preponderant transformation corresponds to the fifth double bond hydrogenation (5.2 TON and 21 h^{-1} TOF; Figure 4; also see Table S4 and Figures S31-S33 in the Supporting Information). Overall, the cumulative TON and TOF for **Ni/Hal** squalene hydrogenation reached 110 and 150.7 h^{-1}, respectively.

With the aim of comparing the efficiency of **Ni/Hal** with common catalysts used in industry, i.e. Ni-Clariant® and Ni-BASF®, we used them for the squalene hydrogenation under the optimized conditions (entries 5-6, Table 1; see Figure S15 in the Supplementary Information for their TEM analyses). To our delight, these commercially available catalysts presented the same results under the selected conditions. With these results in hand, we carried out a scale-up experiment with both catalysts, **Ni/Hal** and Ni-Clariant®, starting with 500 g of squalene. The degree of hydrogenation was comparable for both catalysts, showing a slightly higher iodine value when **Ni/Hal** was used (2.1 vs 1.6 g I_2/100 g of product, for **Ni/Hal** and Ni-Clariant® respectively) (see Table S5 in the Supplementary Information).

In view of the lower reactivity of Co-based catalysts than the analogous on nickel,[47, 48] we used higher metal loading using **Co/Hal** as catalyst (10 mol% of cobalt); at 200 °C under 10 bar H_2,

only 22% conversion was achieved after 4 h, without formation of squalane (entry 7, Table 1). Increasing the pressure up to 40 bar H_2, the activity and chemoselectivity drastically improved (entry 8, Table 1). Lower pressure or lower temperature caused an important detrimental effect (entries 9-10, Table 1). Despite the lower activity of **Co/Hal** versus nickel catalysts towards squalene hydrogenation (for **Ni/Hal**, TON = 20 and for **Co/Hal**, TON = 10; entries 4 and 8, Table 1)), the harsher reaction conditions applied (higher temperature and pressure) offer an alternative to the use of Ni in synthetic applications.

Table 1. Catalytic hydrogenation of squalene by Ni- and Co-based catalysts.[a]

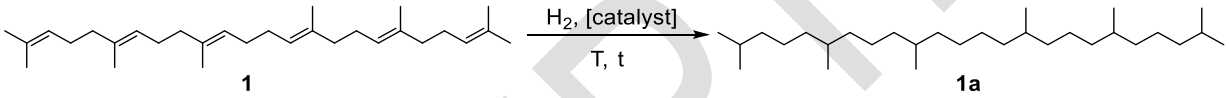

Entry	Catalyst	M mol% (M wt.%)[b]	H_2 (bar)	T (°C)	t (h)	Conv. (yield) (%)[c]
1	**Ni/Hal**	2.3 (0.25)	10	150	4	>99 (19)[d]
2	**Ni/Hal**	2.3 (0.25)	10	200	4	>99 (>99)
3	**Ni/Hal**	2.3 (0.25)	5	200	4	>99 (4)[d]
4	**Ni/Hal**	5 (0.54)	10	150	2	>99 (>99)[e,f]
5	Ni-Clariant®	5 (0.54)	10	150	2	>99 (>99)
6	Ni-BASF®	5 (0.54)	10	150	2	>99 (>99)
7	**Co/Hal**	10 (1.07)	10	200	4	22 (0)[d]
8	**Co/Hal**	10 (1.07)	40	200	2	>99 (>99)[e,g]
9	**Co/Hal**	10 (1.07)	40	150	2	>99 (3)[d]
10	**Co/Hal**	10 (1.07)	25	200	2	>99 (3)[d]

[a] Data from duplicated experiments. [b] M means metal (Ni or Co); metal loading determined by ICP-AES. [c] Determined by GC-FID using dodecane as internal standard. [d] The obtained products mostly correspond to partial hydrogenation of C=C bonds of squalene. [e] TON = mol of consumed

substrate/mol of total metal; TOF = (mol of consumed substrate/mol of total metal)/time. [f] TON = 20; cumulative TON = 110; cumulative TOF = 150.7 h^{-1} (see Table S4). [g] TON = 10.

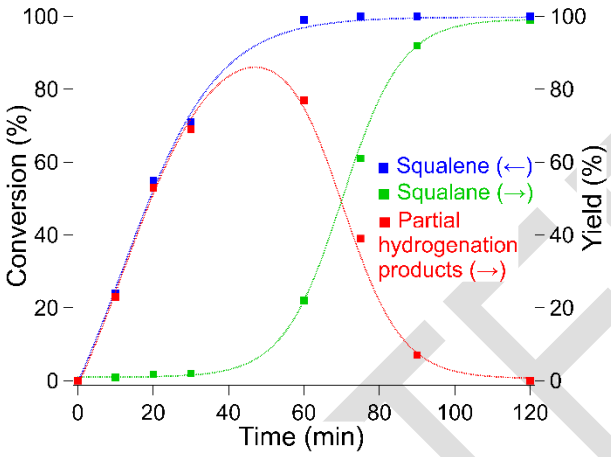

Figure 4. Reaction monitoring of squalene hydrogenation using **Ni/Hal** (5 mol%) at 10 bar and 150 °C, at different times (10, 20, 30, 60, 75, 90 and 120 min). Squalene conversion (■) and squalane yield (■) data points were fitted to sigmoid functions (blue-dotted and green-dotted curves, respectively); the sum of squalene partial hydrogenation intermediates at the aforementioned time points (■) match the red-dotted curve (resulting from the subtraction of the green-dotted sigmoid function from the blue-dotted one).

From a synthetic point of view, both catalysts were applied to obtain squalane in quantitative yields. More remarkable, no metal was detected by ICP-AES on the extracted organic phases, mostly interesting for applications in cosmetics (see Tables S6 and S7 in the Supporting Information). But only **Co/Hal** was robust enough to produce up to 354.6 mg squalane/mg Co (after four consecutive batch runs), in contrast to **Ni/Hal** (only 230.5 mg squalene/mg Ni after two runs), due to the MNPs agglomeration triggering a loss of magnetic properties and thus hampering an efficient recycling (see Figures S16-S20 in the Supplementary Information).

We pursued the catalytic assessment of **Ni/Hal** and **Co/Hal** applying them in the hydrogenation of naturally occurring or biomass derived substrates, such as α-pinene (**2**), ethyl levulinate (**3**), furfural (**4**) and citral (**5**), bearing different unsaturated functional groups (alkenyl, carbonyl or ester groups) (Table 2). α-Pinene was hydrogenated mostly affording the added-value *cis*-pinane (**2a**), with a **2a**/**2b** selectivity up to 95%, which represents a highly selective catalytic systems compared to the literature, most of them using noble based catalysts,[63] and as good as those based on nickel.[64] Both **Ni/Hal** and **Co/Hal** were efficient for the hydrogenation of α-pinene (entries 1-2, Table 2), being more active **Ni/Hal** than **Co/Hal** permitting to work under smoother conditions; however, **Co/Hal** was slightly more selective towards **2a** (92% and 95% **2a**/**2b** selectivity for **Ni/Hal** and **Co/Hal**, respectively).

Table 2. Catalytic hydrogenation of naturally occurring or biomass derivatives.

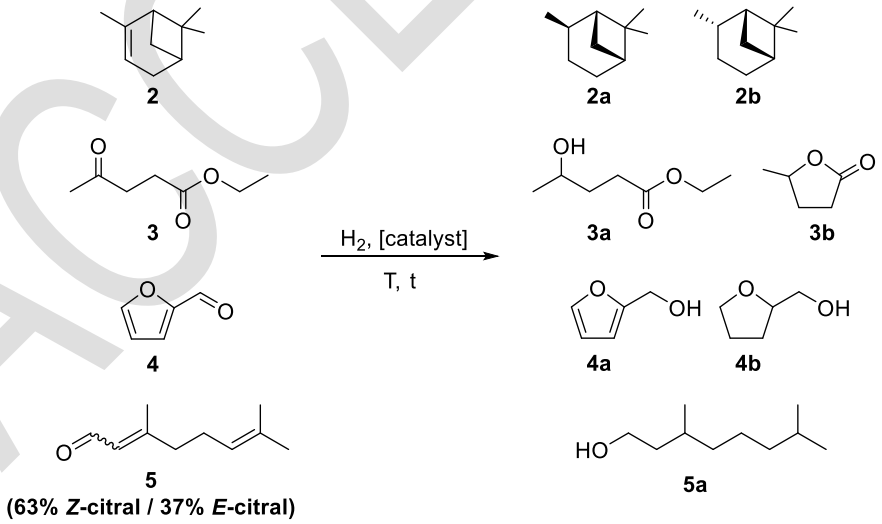

Entry	Catalyst (mol%)[b]	Substrate	H_2 (bar)	T (°C)	t (h)	Conv. (yield) (%)[c]	TON[d]	TOF (h^{-1})[e]

1	**Ni/Hal** (5)	**2**	10	150	2	>99 (96 **2a**, 4 **2b**)	20	10
2	**Co/Hal** (10)	**2**	40	200	2	83 (81 **2a**, 2 **2b**)	8.3	4.1
3	**Ni/Hal** (5)	**3**	10	150	4	>99 (97 **3a**, 3 **3b**)	20	5
4	**Co/Hal** (5)	**3**	40	150	4	>99 (12 **3a**, 88 **3b**)	20	5
5	**Ni/Hal** (5)	**3**	10	200	18	>99 (6 **3a**, 94 **3b**)	20	1.1
6	**Ni/Hal** (5)	**4**	10	150	18	>99 (7 **4a**, 93 **4b**)	20	1.1
7	**Ni/Hal** (2.5)	**4**	10	150	18	>99 (40 **4a**, 60 **4b**)	40	2.2
8	**Co/Hal** (2.5)	**4**	40	200	2	>99 (>99 **4a**)	40	20
9	**Ni/Hal** (5)	**5**	10	150	2	>99 (>99 **5a**)	20	10
10	**Co/Hal** (10)	**5**	40	150	18	>99[f]	10	0.5

[a] Data from duplicated experiments. [b] Metal loading determined by ICP-AES. [c] Determined by GC-FID using dodecane as internal standard. [d] TON = mol of consumed substrate/mol of total Ni. [e] TOF = TON/time. [f] Carried out in heptane, giving a mixture of unsaturated alcohols: 62% citronellol, 29% geraniol and 10% nerol (see Scheme S1 in the Supplementary material).

The hydrogenation of ethyl levulinate led to a mixture of the alcohol **3a** and γ-valerolactone (**3b**), but both catalysts exhibited different chemoselectivity at short reaction time (4 h): while **Ni/Hal** mainly afforded **3a** under relatively smooth conditions (entry 3, Table 2), **Co/Hal** favored the formation of γ-valerolactone (entry 4, Table 2). However, at harsher reaction conditions (200 °C for 18 h), **Ni/Hal** also gave **3b** (94% yield, entry 5, Table 2). The Lewis acidity of the catalyst not only has an impact on lactone formation but also in terms of sensitivity towards catalyst

quenching in the presence of EtOH as concomitant product of the reaction, thus enabling **Co/Hal** to outperform **Ni/Hal** despite using milder reaction conditions.

Furfural hydrogenation catalyzed by **Ni/Hal** and **Co/Hal** also proved the higher activity of **Ni/Hal** compared to **Co/Hal** (entries 6-8, Table 2), trend that permits to obtain selectively the fully reduced alcohol **4b** with **Ni/Hal** (entry 6, Table 2) and furfuryl alcohol (**4a**) with **Co/Hal** (entry 8, Table 2).

Citral (mixture of *E*-citral, named geranial and *Z*-citral, named neral) was fully reduced to the corresponding alcohol by **Ni/Hal** (entry 9, Table 2). However, **Co/Hal** was only active in the presence of a solvent (heptane), reducing the carbonyl functional group, but partially reducing the C=C bonds, yielding a mixture of three alcohols (citronellol, geraniol and nerol; entry 10, Table 2), in agreement with the reluctance observed of **Co/Hal** towards the C=C hydrogenation for squalene, α-pinene and furfural (see above).

The selective hydrogenation of nitriles represents a more challenging task, because a mixture of primary, secondary and tertiary amines can be formed, these last two (including unsaturated ones) arising from condensation reactions between primary or secondary amines with the nitrile or imine functional group. In particular, the formation of primary fatty amines is of great industrial interest (as corrosion inhibitors, surfactants for textile softeners, detergents, and high energy density materials).[65] For that purpose, we have evaluated nitriles bearing long carbon chains (C6-C18), i.e. hexanenitrile (**6**), lauronitrile (**7**) and stearonitrile (**8**). To our delight, we selectively obtained secondary amines using **Ni/Hal** as catalyst and primary amines with **Co/Hal** (Table 3), working under solvent-free conditions and without requiring any additive such as ammonia.[66, 67] For comparative purposes, we evaluated the catalytic behavior of the commercially available catalyst Ni-Clariant® obtaining an undoubtedly lower chemoselectivity in comparison with **Ni/Hal** (entry

7 vs 3, Table 3). The excellent selectivity towards primary fatty amines using the **Co/Hal** catalytic system described herein is comparable to heterogeneous ruthenium–tungsten catalyst on a spinel support ($RuWO_x/MgAl_2O_4$),[68] or molecular Ru coordination complexes (Ru-MACHO and Gusev catalysts).[69] However, **Ni/Hal** shows better selectivity towards secondary amines than noble metal catalysts (Ru, Pd, Pt) described in the literature.[69]

Table 3. Catalytic hydrogenation of fatty nitriles by Ni- and Co-based catalysts.[a]

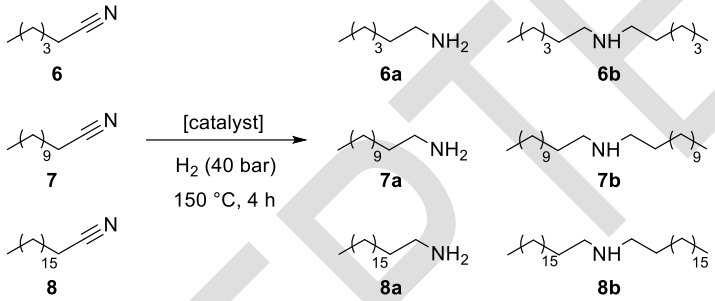

Entry	Catalyst (5 mol% metal)[b]	Substrate	Conversion (%)[c]	Selectivity (a/b)[c]	TON[d]	TOF (h^{-1})[e]
1	**Ni/Hal**	**6**	98	0/92[f]	19.6	4.9
2	**Co/Hal**	**6**	99	90/9	19.8	5.0
3	**Ni/Hal**	**7**	98	4/96	19.6	4.9
4	**Co/Hal**	**7**	97	92/6	19.4	4.9
5	**Ni/Hal**	**8**	99	0/100	19.8	5.0
6	**Co/Hal**	**8**	99	94/3	19.8	5.0
7	Ni-Clariant®	**7**	99	0/64[g]	19.8	5.0

[a] Data from duplicated experiments. [b] M means metal (Ni or Co); metal loading determined by ICP-AES. [c] Determined by ^{1}H NMR using dimethylsulfone as internal standard. [d] TON = mol of consumed substrate/mol of total Ni. [e] TOF = TON/time. [f] 8% of unsaturated secondary and tertiary amines (both saturated and unsaturated ones); see Table S8 in the Supplementary Information. [g] 36% of saturated tertiary amine.

Moreover, the as-prepared catalysts were applied to the upgrading of fatty acid mixtures coming from industrial wastes, namely from agri-food sector (in particular from the duck industry) and wastewater treatments via hydrogenation, with the aim of obtaining more stable saturated fatty compounds. The fatty acid composition of the raw materials is reported in Tables S9-S10 in the Supplementary Information. The selected wastes were esterified with ethanol to obtain the corresponding ethyl ester derivatives, which are not corrosive under H_2 pressure and high temperature in contrast to the analogous carboxylic acids, leading to waste 1 and waste 2 mixtures, used as raw materials for the hydrogenation study (Table 4). Both catalysts led to fully hydrogenated mixtures, being more active the Ni-based catalyst (entries 1 and 3 vs 2 and 4, Table 4; for the composition of the obtained products for each catalyst, see Table S11 in the Supplementary Information).

Furthermore, **Ni/Hal** and **Co/Hal** were also applied in the hydrogenation of olive oil triglycerides (for its composition, see Table S12 in the Supplementary Information), furnishing fully hydrogenated triglycerides of particular interest as emollients and surfactants broadly used in detergents and cosmetic formulations (C18:0, 91%; C16:0, 8%, see Scheme S2 in the Supplementary Information).[70]

Table 4. Catalytic hydrogenation of industrial wastes.[a]

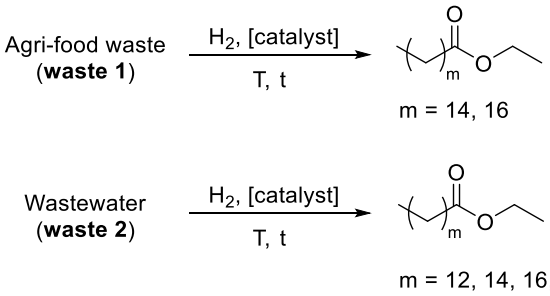

Entry	Catalyst (mol%)[b]	Raw material	H_2 (bar)	T (°C)	t (h)	Conv. (%)[c,d]	TON[e]	TOF[f]
1	**Ni/Hal** (5)	waste 1	10	150	2	>99[g]	20	10
2	**Co/Hal** (10)	waste 1	40	200	4	>99[h]	10	2.5
3	**Ni/Hal** (5)	waste 2	10	150	2	96	19.2	9.6
4	**Co/Hal** (10)	waste 2	40	200	4	>99	10	2.5

[a] Data from duplicated experiments. [b] Metal loading determined by ICP-AES. [c] Conversion stands for the percentage of the C=C bonds hydrogenated; determined by GC-FID using dodecane as internal standard. [d] The composition of the products is collected in Table S11 in the Supplementary Information. [e] TON determined as *mol of consumed substrate/mol of Ni.* [f] TOF determined as *TON/time (h)*. [g] After 1 h of reaction, 70% conversion. [h] After 2 h of reaction, 55% conversion.

Conclusions

Herein, we report the preparation of innovative cobalt and nickel nanocomposite materials with high metal loading (>24 wt.%) immobilized into the inner tubes of unfunctionalized halloysite, exhibiting worthy catalytic activity towards hydrogenation reactions of biomass substrates and industrial wastes. The materials were prepared without addition of stabilizers, leading to metal nanoparticles confined within the halloysite support lumen. Indeed, the electrostatic interactions

between aluminols and metal acetate salts played a crucial role in the immobilization affording aggregates of *ca*. 8 nm and 13 nm mean diameters for **Ni/Hal** and **Co/Hal** nanocomposites, respectively; albeit crystallites of less than 2 nm were determined by PXRD. Thus, the covalent nature of silanol groups present on the outer surface of halloysite nanotubes versus the ionic character of aluminols in the nanotube lumen can be exploited in terms of metal precursors of choice to gain either the immobilization of neutral organometallic complexes on the outer nanotube surface via Van der Waals interactions,[48] or lumen immobilization of cationic metal salts mainly enabled by ionic interactions. The catalytic materials, **Ni/Hal**, and **Co/Hal**, exhibited complementary chemoselectivities in reducing unsaturated functional groups, resulting in selectively added-value compounds based on the choice of metal used. Despite both **Ni/Hal** and **Co/Hal** nanocomposites showed comparable selectivity towards the hydrogenation of C=C bonds, albeit Ni-based catalyst being able to fully hydrogenate furfural into tetrahydrofurfuryl alcohol, whereas Co-based catalytic material was selective in reducing the aldehyde function towards furfuryl alcohol (leaving the furane ring untouched); the most striking chemoselectivity trend was observed in the hydrogenation of nitriles. Thus, a high selectivity towards monoalkylamines could be obtained with **Co/Hal**, whereas the corresponding dialkylamines could be obtained using **Ni/Hal**, probably due its higher Lewis acidity. This differential reactivity between both metal-based catalytic materials can presumably be related with the important difference of the nanoparticles mean size (8.2 nm for **Ni/Hal** *vs* 13.2 nm for **Co/Hal**), prompting an important decrease of the active sites per particle in the case of the cobalt material.

ASSOCIATED CONTENT

Supporting Information. General instrumentation, experimental procedures and materials used; Tables S1-S12, Figures S1-S33, Schemes S1-S2, GC and NMR data for selected compounds.

AUTHOR INFORMATION

Corresponding Authors

Daniel Pla - *Laboratoire Hétérochimie Fondamentale et Appliquée, UMR CNRS 5069, Université Toulouse 3 – Paul Sabatier, 118 route de Narbonne, 31062 Toulouse Cedex 9 (France)*. https://orcid.org/0000-0002-8703-8778 *Email: pla@lhfa.fr

Montserrat Gómez - *Laboratoire Hétérochimie Fondamentale et Appliquée, UMR CNRS 5069, Université Toulouse 3 – Paul Sabatier, 118 route de Narbonne, 31062 Toulouse Cedex 9 (France)*. https://orcid.org/0000-0003-1211-1333 * Email: montserrat.gomez-simon@univ-tlse3.fr

Authors

Alejandro Serrano-Maldonado - *Laboratoire Hétérochimie Fondamentale et Appliquée, UMR CNRS 5069, Université Toulouse 3 – Paul Sabatier, 118 route de Narbonne, 31062 Toulouse Cedex 9 (France)*. https://orcid.org/0000-0003-3076-854X

Jean-Bernard Ledeuil - *Université de Pau et des Pays de l'Adour, E2S UPPA, CNRS, IPREM, Pau (France).* https://orcid.org/0000-0002-7366-2190

Lénaïc Madec - *Institut des Matériaux Jean Rouxel (IMN), CNRS UMR 6502, Université Nantes, 2 rue de la Houssinière BP32229, 44322 Cedex 3 Nantes (France).* https://orcid.org/0000-0002-7681-1681

Romain Rodrigues - *SOPHIM, Rue Pierre-Gilles de Gennes, 04310 Peyruis (France)*

Author Contributions

The manuscript was written through contributions of all authors. All authors have given approval to the final version of the manuscript.

Notes

The authors declare no competing financial interest.

ACKNOWLEDGMENT

We acknowledge Christian Pradel and Sonia Mallet-Ladeira for the (HR)TEM and PXRD analyses respectively and helpful discussions. Authors thank Laetitia Cavaillé and Erwan Trotoux from Sapoval for providing industrial fatty waste samples.

Funding Sources. The Centre National de la Recherche Scientifique (CNRS) and the Université Toulouse 3-Paul Sabatier are gratefully acknowledged for their financial support. Authors thank *Recherche and Societé(s)* program of the Région Occitanie (n°21019948-VADOLI) and SOPHIM (n°249411) for funding this work.

REFERENCES

(1) Zweig, J. E.; Kim, D. E.; Newhouse, T. R. Methods Utilizing First-Row Transition Metals in Natural Product Total Synthesis. *Chem. Rev.* **2017**, *117*, 11680-11752, https://doi.org/10.1021/acs.chemrev.6b00833.

(2) Alig, L.; Fritz, M.; Schneider, S. First-Row Transition Metal (De)Hydrogenation Catalysis Based On Functional Pincer Ligands. *Chem. Rev.* **2019**, *119*, 2681-2751, https://doi.org/10.1021/acs.chemrev.8b00555.

(3) Wei, Y.; Lin, L. Q. H.; Lee, B. C.; Koh, M. J. Recent Advances in First-Row Transition Metal-Catalyzed Reductive Coupling Reactions for π-Bond Functionalization and C-

Glycosylation. *Acc. Chem. Res.* **2023**, *56*, 3292-3312, https://doi.org/10.1021/acs.accounts.3c00531.

(4) Park, S. First-Row Transition Metal-Catalyzed Single Hydroelementation of N-Heteroarenes. *ChemCatChem* **2024**, *16*, e202301422, https://doi.org/https://doi.org/10.1002/cctc.202301422.

(5) Favier, I.; Toro, M.-L.; Lecante, P.; Pla, D.; Gómez, M. Palladium-mediated Radical Homocoupling Reactions: a Surface Catalytic Insight. *Catal. Sci. Technol.* **2018**, *8*, 4766-4773, https://doi.org/10.1039/C8CY00901E.

(6) Hache, E.; Seck, G. S.; Guedes, F.; Barnet, C. Chapter 11: Critical materials - new dependencies and resource curse? In *Handbook on the Geopolitics of the Energy Transition*, Edward Elgar Publishing, 2023; pp 197-216. https://doi.org/10.4337/9781800370432.00017.

(7) Wang, Z.; Chen, Y.; Zhou, F.; Qin, R.; Tian, Y.; Xue, Z.; Mu, T. Upcycling spent lithium-ion battery cathodes into cobalt-polyphenol networks by DES dissolution and solvent-induced crystallization. *Green Chem.* **2024**, *26*, 5988-5996, https://doi.org/10.1039/D4GC01036A.

(8) Kim, K.; Raymond, D.; Candeago, R.; Su, X. Selective cobalt and nickel electrodeposition for lithium-ion battery recycling through integrated electrolyte and interface control. *Nat. Commun.* **2021**, *12*, 6554, https://doi.org/10.1038/s41467-021-26814-7.

(9) He, X. *Solid-State and Polymer Batteries 2023-2033: Technology, Forecasts, Players. Revolutionary approach for the battery business and potential EV game-raisers*. 2023. https://www.idtechex.com/en/research-report/solid-state-and-polymer-batteries-2023-2033-technology-forecasts-players/917 (accessed.

(10) Blakeney, M. *Empowering Europe: Unleashing Cobalt's Potential to Ensure Economic Security and Green Prosperity*. Cobalt Institute, 2024. https://www.cobaltinstitute.org/wp-content/uploads/2024/04/Cobalt-Institute-2024-Manifesto-Unleashing-Cobalts-Potential-To-Ensure-Economic-Security-And-Green-Prosperity.pdf (accessed).

(11) Anderson, J. R. Particle size effects in metal catalysts. *Sci. Prog. (1933-)* **1985**, *69*, 461-484.

(12) Cao, S.; Tao, F.; Tang, Y.; Li, Y.; Yu, J. Size- and shape-dependent catalytic performances of oxidation and reduction reactions on nanocatalysts. *Chem. Soc. Rev.* **2016**, *45*, 4747-4765, https://doi.org/10.1039/c6cs00094k.

(13) Olveira, S.; Forster, S. P.; Seeger, S. Nanocatalysis: academic discipline and industrial realities. *J. Nanotechnol.* **2014**, 324089/324081, https://doi.org/10.1155/2014/324089.

(14) Ndolomingo, M. J.; Bingwa, N.; Meijboom, R. Review of supported metal nanoparticles: synthesis methodologies, advantages and application as catalysts. *J. Mater. Sci.* **2020**, *55*, 6195-6241, https://doi.org/10.1007/s10853-020-04415-x.

(15) Favier, I.; Pla, D.; Gómez, M. Palladium nanoparticles in polyols: synthesis, catalytic couplings and hydrogenations. *Chem. Rev.* **2020**, *120*, 1146-1183, https://doi.org/10.1021/acs.chemrev.9b00204.

(16) Favier, I.; Pla, D.; Gómez, M. Metal-based Nanoparticles Dispersed in Glycerol: an Efficient Approach for Catalysis. *Catal. Today* **2018**, *310*, 98-106, https://doi.org/10.1016/j.cattod.2017.06.026.

(17) Isabelle, F.; David, M.; Emmanuelle, T.; Montserrat, G. Palladium Nanoparticles Applied in Organic Synthesis as Catalytic Precursors. *Curr. Org. Chem.* **2011**, *15*, 3127-3174, https://doi.org/10.2174/138527211797247950.

(18) *Nanomaterials in Catalysis*; Wiley-VCH Verlag GmbH, 2013. https://doi.org/9783527656875.

(19) Henry, C. R. Catalysis by Nanoparticles. In *Nanocatalysis*, Heiz, U., Landman, U. Eds.; Springer Berlin Heidelberg, 2007; pp 245-268. https://doi.org/10.1007/978-3-540-32646-5_3.

(20) Zhang, L.; Zhou, M.; Wang, A.; Zhang, T. Selective hydrogenation over supported metal catalysts: from nanoparticles to single atoms. *Chem. Rev.* **2020**, *120*, 683-733, https://doi.org/10.1021/acs.chemrev.9b00230.

(21) Dabas, S.; Patel, P.; Barik, M.; Subramanian, S.; Prakash, K. S. Chapter 25 - Metal nanoparticles for catalytic hydrogenation reactions. In *Industrial Applications of Nanocrystals*, Mallakpour, S., Hussain, C. M. Eds.; Elsevier, 2022; pp 467-482. https://doi.org/10.1016/B978-0-12-824024-3.00023-3.

(22) Hu, Y.; Liu, M.; Bartling, S.; Lund, H.; Atia, H.; Dyson, P. J.; Beller, M.; Jagadeesh, R. V. A general and robust Ni-based nanocatalyst for selective hydrogenation reactions at low temperature and pressure. *Sci. Adv.* **2023**, *9*, eadj8225, https://doi.org/10.1126/sciadv.adj8225.

(23) Yu, Y.; Hou, Z. Soluble nickel nanoparticles for catalytic hydrogenation. *Curr. Org. Chem.* **2013**, *17*, 336-347, https://doi.org/10.2174/1385272811317040004.

(24) Jaji, N.-D.; Lee, H. L.; Hussin, M. H.; Akil, H. M.; Zakaria, M. R.; Othman, M. B. H. Advanced nickel nanoparticles technology: from synthesis to applications. *Nanotechnol. Rev.* **2020**, *9*, 1456-1480, https://doi.org/10.1515/ntrev-2020-0109.

(25) Anchieta e Silva, F.; Salim, V. M. M.; Rodrigues, T. S. Controlled Nickel Nanoparticles: A Review on How Parameters of Synthesis Can Modulate Their Features and Properties. *AppliedChem* **2024**, *4*, 86-106, https://doi.org/10.3390/appliedchem4010007.

(26) Gao, W.; Liu, S.; Wang, Z.; Peng, J.; Zhang, Y.; Yuan, X.; Zhang, X.; Li, Y.; Pan, Y. Outlook of Cobalt-Based Catalysts for Heterogeneous Hydroformylation of Olefins: From Nanostructures to Single Atoms. *Energy Fuels* **2024**, *38*, 2526-2547, https://doi.org/10.1021/acs.energyfuels.3c03037.

(27) Khodakov, A. Y.; Chu, W.; Fongarland, P. Advances in the Development of Novel Cobalt Fischer-Tropsch Catalysts for Synthesis of Long-Chain Hydrocarbons and Clean Fuels. *Chem. Rev.* **2007**, *107*, 1692-1744, https://doi.org/10.1021/cr050972v.

(28) Harmel, J.; Berliet, A.; Dembele, K.; Marcelot, C.; Gay, A.-S.; Ersen, O.; Maury, S.; Fecant, A.; Chaudret, B.; Serp, P.; et al. A Seed-Mediated Approach for the Preparation of Modified Heterogeneous Catalysts. *ChemCatChem* **2018**, *10*, 1614-1619, https://doi.org/10.1002/cctc.201701860.

(29) Ermakova, M. A.; Ermakov, D. Y. High-loaded nickel–silica catalysts for hydrogenation, prepared by sol–gel: Route: structure and catalytic behavior. *Appl. Catal. A: Gen.* **2003**, *245*, 277-288, https://doi.org/10.1016/S0926-860X(02)00648-8.

(30) Liao, L.; Chen, L.; Ye, R.-P.; Tang, X.; Liu, J. Robust nickel silicate catalysts with high Ni loading for CO_2 methanation. *Chem. Asian J.* **2021**, *16*, 678-689, https://doi.org/10.1002/asia.202001384.

(31) Zhang, Z.; Tian, Y.; Zhang, L.; Hu, S.; Xiang, J.; Wang, Y.; Xu, L.; Liu, Q.; Zhang, S.; Hu, X. Impacts of nickel loading on properties, catalytic behaviors of Ni/γ–Al_2O_3 catalysts and the reaction intermediates formed in methanation of CO_2. *Int. J. Hydrog. Energy* **2019**, *44*, 9291-9306, https://doi.org/10.1016/j.ijhydene.2019.02.129.

(32) Ameen, M.; Azizan, M. T.; Ramli, A.; Yusup, S.; Abdullah, B. The effect of metal loading over Ni/γ-Al_2O_3 and Mo/γ-Al_2O_3 catalysts on reaction routes of hydrodeoxygenation of rubber seed oil for green diesel production. *Catal. Today* **2020**, *355*, 51-64, https://doi.org/10.1016/j.cattod.2019.03.028.

(33) Hermans, L. A. M.; Geus, J. W. Interaction Of Nickel Ions With Silica Supports During Deposition-Precipitation. In *Studies in Surface Science and Catalysis*, Delmon, B., Grange, P., Jacobs, P., Poncelet, G. Eds.; Vol. 3; Elsevier, 1979; pp 113-130. https://doi.org/10.1016/S0167-2991(09)60208-1.

(34) Coenen, J. W. E. Characterization of the standard nickel/silica catalyst EuroNi-1: II. Chemical Aspects: Precipitation, Reduction and Chemical Analysis. *Appl. Catal.* **1989**, *54*, 65-78, https://doi.org/10.1016/S0166-9834(00)82355-6.

(35) Coenen, J. W. E. Characterization of the standard nickel/silica catalyst EuroNi-1: III. Investigations of catalyst structure. *Appl. Catal.* **1991**, *75*, 193-223, https://doi.org/10.1016/S0166-9834(00)83132-2.

(36) Das, T.; Deo, G. Effects of metal loading and support for supported cobalt catalyst. *Catal. Today* **2012**, *198*, 116-124, https://doi.org/10.1016/j.cattod.2012.04.028.

(37) Sun, X.; Suarez, A. I. O.; Meijerink, M.; van Deelen, T.; Ould-Chikh, S.; Zečević, J.; de Jong, K. P.; Kapteijn, F.; Gascon, J. Manufacture of highly loaded silica-supported cobalt Fischer–Tropsch catalysts from a metal organic framework. *Nat. Commun.* **2017**, *8*, 1680, https://doi.org/10.1038/s41467-017-01910-9.

(38) Lira, E.; López, C. M.; Oropeza, F.; Bartolini, M.; Alvarez, J.; Goldwasser, M.; Linares, F. L.; Lamonier, J.-F.; Pérez Zurita, M. J. HMS mesoporous silica as cobalt support for the Fischer–Tropsch Synthesis: Pretreatment, cobalt loading and particle size effects. *J. Mol. Catal. A Chem.* **2008**, *281*, 146-153, https://doi.org/10.1016/j.molcata.2007.11.014.

(39) Camats, M.; Pla, D.; Gómez, M. Copper nanocatalysts applied in coupling reactions. *Nanoscale* **2021**, *13*, 18817-18838, https://doi.org/10.1039/D1NR05894K.

(40) Gonzalez-Arellano, C.; Balu, A. M.; Luque, R.; MacQuarrie, D. J. Catalytically active self-assembled silica-based nanostructures containing supported nanoparticles. *Green Chem.* **2010**, *12*, 1995-2002, https://doi.org/10.1039/c0gc00282h.

(41) Gray-Wannell, N.; Cubillas, P.; Aslam, Z.; Holliman, P. J.; Greenwell, H. C.; Brydson, R.; Delbos, E.; Strachan, L.-J.; Fuller, M.; Hillier, S. Morphological features of halloysite nanotubes as revealed by various microscopies. *Clay Miner.* **2024**, 1-13, https://doi.org/10.1180/clm.2023.37.

(42) Vinokurov, V. A.; Stavitskaya, A. V.; Chudakov, Y. A.; Ivanov, E. V.; Shrestha, L. K.; Ariga, K.; Darrat, Y. A.; Lvov, Y. M. Formation of metal clusters in halloysite clay nanotubes. *Sci. Technol. Adv. Mater.* **2017**, *18*, 147-152, https://doi.org/10.1080/14686996.2016.1278352.

(43) Ouyang, J.; Guo, B.; Fu, L.; Yang, H.; Hu, Y.; Tang, A.; Long, H.; Jin, Y.; Chen, J.; Jiang, J. Radical guided selective loading of silver nanoparticles at interior lumen and out surface of halloysite nanotubes. *Mater. Des.* **2016**, *110*, 169-178, https://doi.org/10.1016/j.matdes.2016.07.127.

(44) Zeng, X.; Wang, Q.; Wang, H.; Yang, Y. Catalytically active silver nanoparticles loaded in the lumen of halloysite nanotubes via electrostatic interactions. *J. Mater. Sci.* **2017**, *52*, 8391-8400, https://doi.org/10.1007/s10853-017-1073-y.

(45) Philip, A.; Lihavainen, J.; Keinanen, M.; Pakkanen, T. T. Gold nanoparticle-decorated halloysite nanotubes - Selective catalysts for benzyl alcohol oxidation. *Appl. Clay Sci.* **2017**, *143*, 80-88, https://doi.org/10.1016/j.clay.2017.03.015.

(46) Zhang, Y.; He, X.; Ouyang, J.; Yang, H. Palladium nanoparticles deposited on silanized halloysite nanotubes: synthesis, characterization and enhanced catalytic property. *Sci. Rep.* **2013**, *3*, 2948, https://doi.org/10.1038/srep02948.

(47) Pérez Alonso, A.; Mauriés, S.; Ledeuil, J.-B.; Madec, L.; Pham Minh, D.; Pla, D.; Gómez, M. Nickel Nanoparticles Immobilized on Pristine Halloysite: An Outstanding Catalyst for Hydrogenation Processes. *ChemCatChem* **2022**, *14*, e2022007, https://doi.org/10.1002/cctc.202200775.

(48) Serrano-Maldonado, A.; Bendounan, A.; Silly, M. G.; Pla, D.; Gómez, M. Selective catalytic hydrogenation of fatty acids with cobalt-halloysite nanocomposites for waste valorization. *ACS Appl. Nano Mater.* **2023**, *6*, 11317–11326, https://doi.org/10.1021/acsanm.3c01361.

(49) Zhu, Z.; Ding, D.; Zhang, Y.; Zhang, Y. Preparation of Ni, CoO-supported halloysite nanotube catalyst and its application in the hydrogenation of furfural to furfuryl alcohol. *Appl. Clay Sci.* **2020**, *196*, 105761, https://doi.org/10.1016/j.clay.2020.105761.

(50) Glotov, A.; Vutolkina, A.; Pimerzin, A.; Vinokurov, V.; Lvov, Y. Clay nanotube-metal core/shell catalysts for hydroprocesses. *Chem. Soc. Rev.* **2021**, *50*, 9240-9277, https://doi.org/10.1039/D1CS00502B.

(51) Pasbakhsh, P.; De Silva, R.; Vahedi, V.; Jock Churchman, G. Halloysite nanotubes: prospects and challenges of their use as additives and carriers – A focused review. *Clay Miner.* **2018**, *51*, 479-487, https://doi.org/10.1180/claymin.2016.051.3.15.

(52) Jock Churchman, G.; Pasbakhsh, P.; Hillier, S. The rise and rise of halloysite. *Clay Miner.* **2018**, *51*, 303-308, https://doi.org/10.1180/claymin.2016.051.3.00.

(53) Gray-Wannell, N.; Holliman, P. J.; Greenwell, H. C.; Delbos, E.; Hillier, S. Adsorption of phosphate by halloysite (7 Å) nanotubes (HNTs). *Clay Miner.* **2020**, *55*, 184-193, https://doi.org/10.1180/clm.2020.24.

(54) Sadjadi, S. Halloysite-based hybrids/composites in catalysis. *Appl. Clay Sci.* **2020**, *189*, 105537, https://doi.org/10.1016/j.clay.2020.105537.

(55) Jiang, D.; Jing, H.; Liu, Z.; Jia, C.; Liu, Q. Natural Halloysite Nanotube as a Spatially Confined Nanoreactor for Improving Photocatalytic Performance. *J. Phys. Chem. C* **2021**, *125*, 15316-15323, https://doi.org/10.1021/acs.jpcc.1c04065.

(56) Li, Y.; Yuan, X.; Jiang, L.; Dai, H.; Zhao, Y.; Guan, X.; Bai, J.; Wang, H. Manipulation of the halloysite clay nanotube lumen for environmental remediation: a review. *Environ. Sci.: Nano* **2022**, *9*, 841-866, https://doi.org/10.1039/D1EN01032H.

(57) Massaro, M.; Colletti, C. G.; Lazzara, G.; Milioto, S.; Noto, R.; Riela, S. Halloysite nanotubes as support for metal-based catalysts. *J. Mater. Chem. A* **2017**, *5*, 13276-13293, https://doi.org/10.1039/c7ta02996a.

(58) Sanchez-Ballester, N. M.; Ramesh, G. V.; Tanabe, T.; Koudelkova, E.; Liu, J.; Shrestha, L. K.; Lvov, Y.; Hill, J. P.; Ariga, K.; Abe, H. Activated interiors of clay nanotubes for agglomeration-tolerant automotive exhaust remediation. *J. Mater. Chem. A* **2015**, *3*, 6614-6619, https://doi.org/10.1039/c4ta06966h.

(59) Pérez Alonso, A.; Serrano-Maldonado, A.; Ledeuil, J.-B.; Madec, L.; Minh, D. P.; Pla, D.; Gómez, M. Advanced Nickel-based Catalytic Materials on Hydroxyapatite: Effect of the Metal Particle Size on Tri-reforming of Methane. *ACS Sustainable Resour. Manage.* **2024**, https://doi.org/10.1021/acssusresmgt.3c00099.

(60) Mamontova, E.; Trabbia, C.; Favier, I.; Serrano-Maldonado, A.; Ledeuil, J.-B.; Madec, L.; Gómez, M.; Pla, D. Novel Catalyst Composites of Ni- and Co-Based Nanoparticles Supported on Inorganic Oxides for Fatty Acid Hydrogenations. *Nanomaterials* **2023**, *13*, 1435, https://doi.org/10.3390/nano13091435.

(61) Ciriminna, R.; Pandarus, V.; Beland, F.; Pagliaro, M. Catalytic Hydrogenation of Squalene to Squalane. *Org. Process Res. Dev.* **2014**, *18*, 1110-1115, https://doi.org/10.1021/op5002337.

(62) Kim, S.-K.; Karadeniz, F. Biological importance and applications of squalene and squalane. *Adv. Food Nutr. Res.* **2012**, *65*, 223-233, https://doi.org/10.1016/B978-0-12-416003-3.00014-7.

(63) Ndongou Moutombi, F. J.; Selka, A.; Fabiano-Tixier, A.-S.; Foucher, D.; Clarisse, O.; Chemat, F.; Touaibia, M. Highly selective solvent-free hydrogenation of pinenes to added-value cis-pinane. *C. R. Chim.* **2018**, *21*, 1035-1042, https://doi.org/10.1016/j.crci.2018.09.002.

(64) Hu, S.; Wang, L.; Chen, X.; Wei, X.; Tong, Z.; Yin, L. The conversion of α-pinene to cis-pinane using a nickel catalyst supported on a discarded fluid catalytic cracking catalyst with an ionic liquid layer. *RSC Adv.* **2019**, *9*, 5978-5986, https://doi.org/10.1039/c9ra00675c.

(65) Chen, T.; Sun, H.; Mu, P.; Zhu, Z.; An, J.; Liang, W.; Li, A. Fatty amines as a new family of organic phase change materials with exceptionally high energy density. *Sol. Energy Mater. Sol. Cells* **2020**, *206*, 110340, https://doi.org/10.1016/j.solmat.2019.110340.

(66) Behr, A.; Seidensticker, T. The Basics of Oleochemistry - Basic Oleochemicals. In *Chemistry of Renewables*, Springer Berlin Heidelberg, 2020; pp 37-60. https://doi.org/10.1007/978-3-662-61430-3_3.

(67) Ma, Z.; Chandrashekhar, V. G.; Zhou, B.; Alenad, A. M.; Rockstroh, N.; Bartling, S.; Beller, M.; Jagadeesh, R. V. Stable and reusable Ni-based nanoparticles for general and selective hydrogenation of nitriles to amines. *Chem. Sci.* **2022**, *13*, 10914-10922, https://doi.org/10.1039/D2SC02961H.

(68) Coeck, R.; De Vos, D. E. One-pot reductive amination of carboxylic acids: a sustainable method for primary amine synthesis. *Green Chem.* **2020**, *22*, 5105-5114, https://doi.org/10.1039/D0GC01441A.

(69) Hinzmann, A.; Gröger, H. Selective Hydrogenation of Fatty Nitriles to Primary Fatty Amines: Catalyst Evaluation and Optimization Starting from Octanenitrile. *Eur. J. Lipid Sci. Technol.* **2020**, *122*, 1900163, https://doi.org/10.1002/ejlt.201900163.

(70) Scharnagl, F. K.; Hertrich, M. F.; Ferretti, F.; Kreyenschulte, C.; Lund, H.; Jackstell, R.; Beller, M. Hydrogenation of terminal and internal olefins using a biowaste-derived heterogeneous cobalt catalyst. *Sci. Adv.* **2018**, *4*, eaau1248/1241, https://doi.org/10.1126/sciadv.aau1248.

TOC/Abstract Graphic